Journal of Structural Geology, Vol. 15, No. 2, pp. 207 to 218, 1993
Printed in Great Britain

0191-8141/93 $06.00+0.00
© 1993 Pergamon Press Ltd

Strain factorization by identical finite increments and its use

RICHARD T. CHEN

Department of Earth and Space Sciences, University of California, Los Angeles, CA 90024, U.S.A.

(*Received* 24 *June* 1991; *accepted in revised form* 17 *July* 1992)

Abstract—Progressive deformation of layered rocks, up to their present finite strain and bedding attitudes, is simulated by an identical-increment-path model. A deformation matrix connecting the initial and deformed states is formulated with the conceptual help of a hypothetical three-step deformation path. Two sequential non-coaxial rigid-body rotations bring an original horizontal bed to a pre-strain attitude; a pure shear follows the rotations. Thus, the deformation matrix is calculated by premultiplying the matrices representing the three stages of deformation. Sixteen identical tectonic deformation increments are then obtained by four times sequentially extracting the 'square-root' of that deformation matrix.

The method has been applied to the Campbell block, a Late Jurassic fault-bounded turbidite sliver in the northern Sierra Nevada, California. The block was deformed into a train of folds during the Nevadan orogeny. Fourteen oriented samples were collected for March strain measurements. Based on the strains and bedding attitudes, the block was divided into 11 deformation bands, of three types. By applying the proposed model to the Campbell block, it was found that the deformation style of the block consists of a non-coaxial deformation path. The regional strain is accommodated among the several deformation bands by strain partitioning; the collective deformation indicated by this model is transpressional.

INTRODUCTION

THE concept of progressive deformation has been introduced to structural geologists by Flinn (1962); an original sphere within a rock is deformed continuously and progressively to form a series of different ellipsoids. The natural occurrence of such a history in rocks is manifest by the growth patterns of curved fibroid crystals in extension veins or in 'pressure shadows' (Durney & Ramsay 1973, Ramsay & Huber 1983, pp. 235–280, Passchier 1987). Ramsay (1967) and Elliott (1972) elaborated Flinn's (1962) progressive deformation path and represented it mathematically by matrix algebra in a fixed external co-ordinate frame. In recent years, the concept has been applied to both mathematical forward modelling of deformation histories (Ramberg 1975, Ramberg & Ghosh 1977, Means *et al.* 1980, McKenzie & Jackson 1983, Schwerdtner & Gapais 1983, Sanderson & Marchini 1984, Shore & Duncan 1984, Ellis & Watkinson 1987) and regional strain analysis (Coward & Potts 1983, Odling 1984, Schultz-Ela & Hudleston 1991). Among the existing mathematical models, some (Means *et al.* 1980, McKenzie & Jackson 1983, Ellis & Watkinson 1987) assume complete information on both the temporal and spatial factors, and adopt the approach of infinitesimal deformation; they derive a rate-of-deformation tensor. For most geological cases, unfortunately, the evidence for timing and spatial constraints is incomplete, and no rate-of-deformation tensors can be found. Those approaches employing finite-deformation (Ramberg 1975, Ramberg & Ghosh 1977, Shore & Duncan 1984) are forward models; for application to geological cases (Coward & Potts 1983, Odling 1984, Schultz-Ela & Hudleston 1991) they rely on trial-and-error fitting routines.

In this study, I take a finite-deformation approach and introduce a routine to calculate deformation increments directly. Based on the present finite strain and bedding attitude of a layered rock, a deformation matrix which does account for any change of shape and rotation but not for translation is derived from the model. The progressive deformation is segmented into small but finite increments, and for mathematical simplicity all increments are assumed to be identical. Such a deformation path can be calculated by sequential premultiplication of every intermediate, cumulative deformation matrix with another incremental finite deformation matrix. A deformation style is obtained by examining each incremental finite deformation matrix and resolving it into an incremental pure shear and an incremental rigid-body rotation by polar decomposition.

A sliver of Jurassic turbidite near Colfax, California (Fig. 1) (called Campbell block hereafter), bounded by high-angle reverse faults (Day *et al.* 1985), is used as an example. This domain has been deformed into a train of folds. An attempt to elucidate the nature of this event, at least to a first order of approximation, is the subject of the following investigation.

DEFORMATION MATRIX

A deformation matrix, referred to a given co-ordinate system, describes an unique finite deformation; it links the undeformed to the deformed state of a rock (e.g. Flinn 1979). The deformed state described by the matrix can be reached by an infinite number of paths, only one of which, however, actually occurred (e.g. Elliott 1972). In the following derivation and example, all vectors, matrices, tensors and bedding attitudes are referred to the current Cartesian geographic co-ordinates, north, east and down (Fig. 2a). Layered sedimentary rocks are

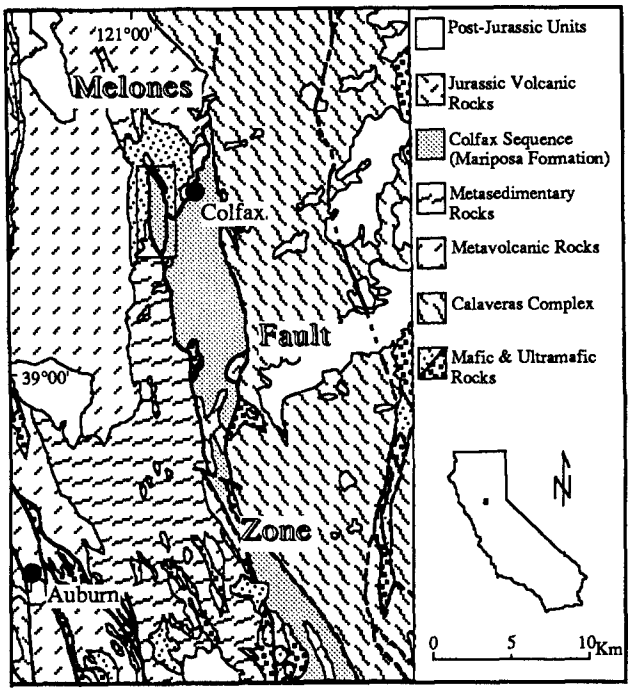

Fig. 1. Simplified geological map of the Auburn–Colfax region, northern California. Modified from the 1:250,000 Sacramento Quadrangle (Wagner *et al.* 1981), and Chico Quadrangle (Burnett & Jennings 1962), Geologic Map of California. Box indicates position of the Campbell block.

here assumed to have been laid down horizontally (Fig. 2a); in their final states they have a measurable total ·in, and their bedding attitudes can be observed at the ·ıcrop (Fig. 2f).

To formulate an unambiguous deformation matrix **D** for such rocks, I adapt a conceptual hypothetical deformation path (Fig. 2) also used by Cogné & Perroud (1985) to restore the paleomagnetic direction of rocks. The path consists of a pure shear component expressed by a matrix **S** following a rigid-body rotation expressed by a matrix **Z**. Based on this path, the matrices have the relationship (equivalent to the left polar decomposition of Elliott 1970):

$$\mathbf{D} = \mathbf{S}\,\mathbf{Z}. \qquad (1)$$

The pure shear component **S** can be obtained by any one of various strain estimating methods (Ramsay & Huber 1983, pp. 167–214); here, the March model (1932) has been used. For his model one assumes that all components of a sample are affected uniformly by a homogeneous strain (Oertel 1983). The model allows one to estimate the strain from its geometrical consequence, the modified orientation of the rock's linear or planar markers (Owens 1973, Chen & Oertel 1991). The strain estimated with the March model is called March strain. In order to determine the rotation **Z**, one has to find the orientation of an original bed (a material plane), defined by its original attitude (assumed horizontal) and by the azimuth of at least one material line in the bedding plane (say one originally oriented N–S), and the attitudes of the same material plane (known) and the same line (usually unknown) in that plane after the hypothetical pre-strain rotation **Z**. Unit vectors, ${}^{d}\mathbf{1}$, ${}^{z}\mathbf{1}$ and ${}^{o}\mathbf{1}$, are used to represent the poles of beds in the observed, the hypothetical pre-strain, and the original horizontal attitudes. The bedding pole ${}^{o}\mathbf{1}$ thus has the components [0.0, 0.0, 1.0]. The hypothetical pre-strain pole ${}^{z}\mathbf{1}$ can be determined (Owens 1973) by:

$${}^{z}\mathbf{1} = k\,{}^{d}\mathbf{1}\,\mathbf{S}, \qquad (2)$$

where the factor k scales the product of ${}^{d}\mathbf{1}$ and **S** to unity. The rigid-body rotation **Z** can be further decomposed

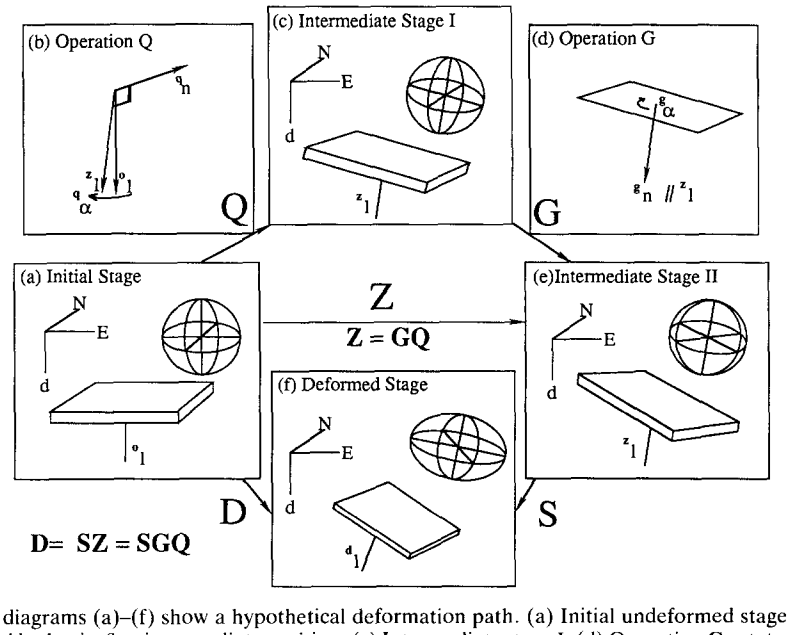

Fig 2. Schematic diagrams (a)–(f) show a hypothetical deformation path. (a) Initial undeformed stage. (b) Operation **Q** rotates a horizontal bed to its first intermediate position. (c) Intermediate stage I. (d) Operation **G** rotates bedding about an axis parallel to the bedding pole of the first intermediate stage. (e) Intermediate stage II. (f) The final deformed stage after strain **S**.

into two non-coaxial rotations (Figs. 2b & d), **G** and **Q**, such that:

$$\mathbf{Z} = \mathbf{G}\,\mathbf{Q}. \tag{3}$$

Rotation matrix **Q** is taken to rotate ${}^{o}\mathbf{1}$ by an angle ${}^{q}\alpha$ to ${}^{z}\mathbf{1}$, about an axis ${}^{q}\mathbf{n}$ which is normal to both ${}^{o}\mathbf{1}$ and ${}^{z}\mathbf{1}$ (Fig. 2b). Because the pole ${}^{o}\mathbf{1}$ is vertical, the axis ${}^{q}\mathbf{n}$ is horizontal and can be determined by the cross product of ${}^{o}\mathbf{1}$ and ${}^{z}\mathbf{1}$. Substituting the values of ${}^{q}\alpha$ and ${}^{q}\mathbf{n}$ into equation (A3) (Appendix A), the rotation matrix **Q**, representing the horizontal-axis component of rotation **Z**, is determined. Rotation matrix **G**, the normal-axis component of rotation **Z**, assumed to be following rotation **Q**, rotates by an angle of ${}^{g}\alpha$ about a pole ${}^{z}\mathbf{1}$ (Fig. 2d). Because the orientation of a material plane is insufficiently determined by its pole alone, the angle ${}^{g}\alpha$ is commonly uncertain. Given a bedding attitude after a known total strain, and assuming that the bed was deposited horizontally, there exists a whole family of deformation matrices as a function of the variable ${}^{g}\alpha$ such that:

$$\mathbf{D} = \mathbf{D}({}^{g}\alpha) = \mathbf{S}\,\mathbf{G}({}^{g}\alpha)\,\mathbf{Q}. \tag{4}$$

To determine a particular deformation matrix from this family $\mathbf{D}({}^{g}\alpha)$, information of the initial and deformed orientations of a material line on the bedding plane is required. Such information may be extracted from deflected remanent magnetic vectors (MacDonald 1980, Cogné & Perroud 1987); provided one knows how the vectors respond to deformation (Borradaile 1991, Borradaile & Mothersill 1991). Otherwise, an assumption needs to be made (see 'Application').

EQUAL-INCREMENT DEFORMATION MODEL

Because March strain, used in this study, measures the total strain suffered by a rock since it was deposited (Oertel 1983, Chen & Oertel 1989), compaction is treated as part of the deformation. The working deformation model is built on the assumption that after the compaction, **C**, the rock was deformed sequentially by a number of identical deformation increments ${}^{i}\mathbf{D}$. Theoretically, to approach an infinitesimal deformation and to yield a truely progressive deformation, the size of increments should approach zero and their number infinity (Ramberg 1975). In this study, to compromise between excessive round-off errors caused by too many repeated computations and unacceptable increment size, I found a number of 16 increments to be the optimal. The model can be expressed by the matrix equation:

$$\mathbf{D} = ({}^{i}\mathbf{D})^{16}\ \mathbf{C}. \tag{5}$$

Assuming that compaction occurred in a confined basin, the compaction stretch tensor is uniaxial with its shortening axis vertical. Because March strains are conventionally stated as constant-volume strains, the stretch tensor, C_{ij}, for March compaction is deviatoric:

$$[C_{ij}(x)] = \begin{bmatrix} x^{-1/3} & 0 & 0 \\ 0 & x^{-1/3} & 0 \\ 0 & 0 & x^{-1/3} \end{bmatrix} \begin{bmatrix} 1 & 0 & 0 \\ 0 & 1 & 0 \\ 0 & 0 & x \end{bmatrix} = \begin{bmatrix} x^{-1/3} & 0 & 0 \\ 0 & x^{-1/3} & 0 \\ 0 & 0 & x^{2/3} \end{bmatrix}. \tag{6}$$

The matrix $C_{ij}(x)$ is a function of the variable compacted vertical elongation, x, which is smaller than unity. By removing the compaction from the total deformation **D** in equation (5), the tectonic deformation matrix ${}^{t}\mathbf{D}$ is calculated as follows:

$${}^{t}\mathbf{D} = \mathbf{D}\,\mathbf{C}^{-1} = ({}^{i}\mathbf{D})^{16}. \tag{7}$$

The identical tectonic deformation increments are obtained by four times sequentially extracting the 'square-root' (see procedure in Appendix B) of the tectonic deformation matrix:

$${}^{i}\mathbf{D} = ({}^{t}\mathbf{D})^{1/16} = ({}^{t}\mathbf{D})^{(1/2)^4}. \tag{8}$$

By substituting equations (4) and (6) into equation (7), then substituting the result into equation (8), one obtains:

$${}^{i}\mathbf{D} = (\mathbf{S}\,\mathbf{G}({}^{g}\alpha)\,\mathbf{Q}\,\mathbf{C}(x)^{-1})^{(1/2)^4}. \tag{9}$$

Equation (9) indicates that under insufficient constraints each member of a family of different matrices (9) could potentially be a deformation increment for the model.

Once a deformation increment ${}^{i}\mathbf{D}$ is determined, its nature can be analyzed by right or left polar decomposition (p. 12 in Spencer 1980), which decomposes the increment into sub-increments of pure shear, ${}^{i}\mathbf{U}$ or ${}^{i}\mathbf{V}$, and of rigid-body rotation, ${}^{i}\mathbf{R}$. Right polar decomposition produces:

$${}^{i}\mathbf{D} = {}^{i}\mathbf{R}\ {}^{i}\mathbf{U}. \tag{10}$$

Left polar decomposition produces:

$${}^{i}\mathbf{D} = {}^{i}\mathbf{V}\ {}^{i}\mathbf{R}. \tag{11}$$

Because the deformation increments ${}^{i}\mathbf{D}$ are small, the two pure shear increments ${}^{i}\mathbf{U}$ and ${}^{i}\mathbf{V}$ are approximately equal; in this study, I arbitrarily use the right polar decomposition. The principal values and axes of ${}^{i}\mathbf{U}$ can be obtained by using the procedure for analyzing the eigenvalues and eigenvectors of a tensor described by Nye (1957, pp. 41–43). The rotation axis and amount of rotation by the rigid-body rotation ${}^{i}\mathbf{R}$ can be calculated by equations (A4) and (A5) in Appendix A.

DEFORMATION SIMULATION

A rock unit containing beds that were initially horizontal, deformed according to the proposed model, goes through 32 intermediate bedding attitudes and states of strain. The passage from the initial to the first incremental stage is the compaction **C**, described by a deformation matrix, $\mathbf{D}_1$:

$$\mathbf{D}_1 = \mathbf{C}. \quad (12)$$

The second incremental stage results from the rock being deformed by a finite increment of pure shear ${}^{i}\mathbf{U}$, and it is described by a deformation matrix, $\mathbf{D}_2$:

$$\mathbf{D}_2 = {}^{i}\mathbf{U}\,\mathbf{D}_1 = {}^{i}\mathbf{U}\,\mathbf{C}. \quad (13)$$

In the third stage an incremental rigid-body rotation ${}^{i}\mathbf{R}$ follows the strain ${}^{i}\mathbf{U}$, and the third-stage deformation matrix $\mathbf{D}_3$ is therefore the result of $\mathbf{D}_2$ being premultiplied by ${}^{i}\mathbf{R}$:

$$\mathbf{D}_3 = {}^{i}\mathbf{R}\,\mathbf{D}_2 = {}^{i}\mathbf{R}\,{}^{i}\mathbf{U}\,\mathbf{C}. \quad (14)$$

For the fourth stage, the new deformation matrix, $\mathbf{D}_4$, becomes:

$$\mathbf{D}_4 = {}^{i}\mathbf{U}\,\mathbf{D}_3 = {}^{i}\mathbf{U}\,{}^{i}\mathbf{R}\,{}^{i}\mathbf{U}\,\mathbf{C}, \quad (15)$$

and so on. The 32 intermediate cumulative deformation matrices $\mathbf{D}_j$ (j varies from 1 to 32) can be calculated as above. The state of cumulative strain, $\mathbf{U}_j$, is determined by right polar decomposition of the corresponding deformation matrix $\mathbf{D}_j$.

The intermediate bedding attitudes are obtained by following the orientations of two deformed material lines in the original bedding plane through the stages; one, initially parallel to the present geographic north, is represented by a vector ${}^{N}\mathbf{1}$; another, initially parallel to present east, is represented by ${}^{E}\mathbf{1}$. Their subsequent orientations, ${}^{N}\mathbf{1}_j$ and ${}^{E}\mathbf{1}_j$, are calculated as:

$${}^{N}\mathbf{1}_j = \mathbf{D}_j\,{}^{N}\mathbf{1}^{T}, \quad (16)$$

and

$${}^{E}\mathbf{1}_j = \mathbf{D}_j\,{}^{E}\mathbf{1}^{T}. \quad (17)$$

The poles ${}^{P}\mathbf{1}_j$ to the intermediate bedding attitudes are the cross products of ${}^{N}\mathbf{1}_j$ with ${}^{E}\mathbf{1}_j$.

The calculated path should closely mimic the actual deformation path of an isotropic rock deformed under steady-state conditions because the total deformation matrix is taken to be the cumulative result of identical increments. If, however, the rock is anisotropic or suffers strain softening or hardening during its deformation history, the calculated path is only an approximation. The pure shear components of the path, ${}^{i}\mathbf{U}$, are the incremental responses of a hypothetical isotropic rock subjected to steady-state conditions.

APPLICATION

In the following, the model is applied to the Campbell block to investigate the nature and evolution of its deformation. The block may, to a first order of approximation, be considered a single train of folds, and based on bedding attitudes and strain measurements it was divided into 11 deformation bands, of three types. Separate analysis of the data from each type produces no unique solution but a whole family of deformation matrices (equation 4), and thus of tectonic deformation increments (equation 9). Both these families are functions of the unknown compaction factor, x (equation 6), and the unknown normal-axis component of initial rotation ${}^{g}\alpha$ (equation 4). The most plausible sets of deformation matrices for the three band types were selected from the corresponding families by two additional assumptions. First, rocks throughout the block were assumed to have been equally compacted, and secondly, spatial variations of incremental pure shear within each type of deformation band were taken to be minimal.

Geological setting

The Campbell block, located 2 km west of the town of Colfax, California, U.S.A., is 5 km long from north to south and 1 km wide (Fig. 3). It is bounded by the Milk Ranch thrust and Bear River fault (Chandra 1961), the latter forming the western boundary of the Melones fault zone (Fig. 1). The Milk Ranch thrust juxtaposed the Campbell block to the older mafic plutonic rocks of the Lake Combie Complex on the east (Day *et al.* 1985); the Bear River fault brought the Paleozoic Clipper Gap Formation into contact with the western boundary of the block. Both faults have been shown to be W-directed backthrusts (Moores & Day 1984, Day *et al.* 1985), representing the latest Nevadan movements between 160 and 150 Ma (Day *et al.* 1985).

Most rocks in the Campbell block were originally correlated to the Mariposa Formation of the southern Sierra Nevada by Chandra (1961) and were mapped as Late Jurassic turbidites consisting of interbedded conglomerate, sandstone, shale, and minor tuff by Tuminas (1983). From fossil evidence (Imlay 1961), the rocks range from early Callovian to late Oxfordian (169–156 Ma). Sedimentary structures and sedimentary facies indicate that the Colfax sequence was probably deposited in relatively small elongated basins (Day *et al.* 1985).

The Campbell block was later, during the Nevadan orogeny (Day *et al.* 1985), deformed into a train of folds in a tectonic setting still under debate. A convergent margin operating in the Nevadan orogeny has been proposed by a school of workers (Hamilton 1969, Moores 1972, Burchfiel & Davis 1975, Schweickert & Cowan 1975, Ingersoll & Schweickert 1986); but a contradictory transform model was preferred by Saleeby *et al.* (1978) and Harper *et al.* (1985).

Fold train geometry

The fold train in the block consists of a main, open syncline flanked by series of tight folds on both its east and west sides (Fig. 3). The axial traces of these folds share an approximately NNW trend at an acute angle (10–30°) to the boundary faults (Fig. 3). The main syncline is nearly cylindrical, and the flanking folds have chevron shapes. Their average fold axis can therefore be calculated by Ramsay's procedure (1967, pp. 18–19), to trend 331° and plunge 33° (Fig. 4). The bedding attitudes in the block can be grouped into three sets; they are a steeply E-dipping (E-set), a shallowly NW-dipping (N-

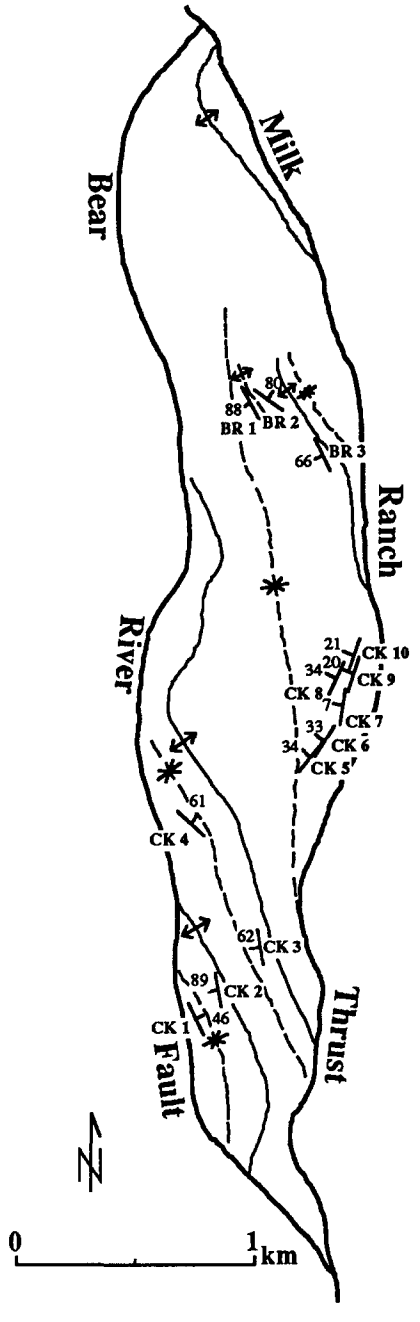

Fig. 3. Structural map of the Campbell block, modified from Chandra (1961). Traces of anticlinal and synclinal axial hinge planes are indicated. Centers of attitude symbols indicate sample locations.

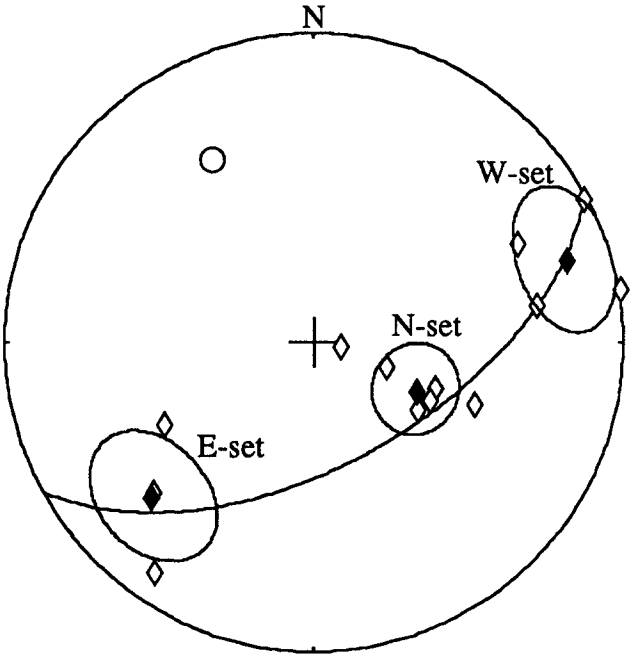

Fig. 4. Lower-hemisphere equal-area projection of the π-diagram for the train of folds in the Campbell block. Circle: fold axis. Open diamonds: poles to bedding. Filled diamonds: average poles. E, N, W: E-, N- and W-sets. Small-circles: 1 – σ scattering from average poles (Scheidegger 1965). Great-circle: normal to fold axis.

set), and a steeply W-dipping (W-set) set with average attitudes of 136°/62°E, 25°/30°NW, and 161°/77°W, respectively, calculated by Scheidegger's (1965) method (Fig. 4). The N-set represents the bottom of the main syncline; the W- and E-sets are representative of the limbs of the multiple flanking anticlines and synclines. The hinge areas of the flanking folds are commonly obscured by erosion or by vegetation; no continuous key bed can be traced along the fold train. The main, open syncline has no discrete hinge area.

Strains at the sample points

Fourteen oriented samples were collected away from hinge areas at various stratigraphic levels; their locations and attitudes are indicated on Fig. 3. They are interlayered siltstones and shales, with the thickness of individual layers varying from 2 to 20 mm. The contacts between these layers are disturbed, possibly by a combination of sedimentary and tectonic processes.

The preferred orientation of chlorite grains in the shale interlayers between siltstones was measured, and the March model (1932) for strain estimation was applied. The procedure to estimate the strain is a computer-aided least-squares fitting routine (Chen & Oertel 1991). It derives the March strain from the angular density distribution function (ADF of Owens 1973) of chlorite basal planes; the ADF was mapped with an automated pole-figure goniometer in the transmission mode (Wenk 1985). The data set consists of 420 X-ray intensities taken at various sample orientations. Table 1 lists the principal strain values and directions referred to geographic co-ordinates. The principal strain directions are scattered within three sets of clusters (Figs. 5a–c). Samples belonging to the same clusters of principal strain directions also share a cluster of bedding attitudes (Fig. 4).

Model fitting

In analogy to Cobbold's (1977) concept of deformation bands, the Campbell block was divided into 11 bands separated by the trace of axial surfaces (Fig. 6). The division was based on the coextensive grouping of both the bedding attitudes and the principal strain directions into three types. Abandoning Cobbold's assumption of continuity across band boundaries, the model treats them as mathematical discontinuity surfaces, as do Johnson & Ellen (1974). Two considerations justify this relaxation. First, by stress concentration a folded

layer commonly yields preferentially in the hinge area (Biot 1961). Secondly, diffusional mass transport at a macroscopic scale (Fletcher 1982) may cause local volume changes in the hinge areas. Because each limb of the fold train remains to be planar, at the regional scale, the rock in each deformation band away from the hinge areas, must be homogeneously deformed with only local perturbations; their total strains and perturbations can be represented by the average strains and by the strain dispersions in each of the three sets.

The average strain was calculated by taking the arithmetic mean of the natural strain tensors for each of the sets and then converting those to conventional strain (Oertel *et al.* 1989). Table 2 lists the mean principal values and directions, and Figs. 5(a)–(c) show principal directions for the complete three sets and their means. The strain dispersion, $\pm S$, in each set is evaluated by the equation following:

$$\pm S = \sqrt{\frac{\sum_{ij}^{33} \frac{\sum_k^n (\overline{S_{ij}} - {}^kS_{ij})_k^2}{n-1}}{9}}, \qquad (18)$$

where $\overline{S_{ij}}$ are the components of the average strain, and ${}^kS_{ij}$ are the components of the k-th strain tensor in a sample population of size n. The dispersion in deformation bands of the same type reflects either measurement uncertainty or local inhomogeneities (Cobbold 1977). In the latter case, the dispersion may have been caused by local rheological contrasts, by local stress concentrations, or by variations of the structural level from which the samples were taken.

From known mean March strains and bedding attitudes, guessed normal-axis components of initial rotation, ${}^g\alpha_e$, ${}^g\alpha_n$ and ${}^g\alpha_w$, and compaction factors, x, for each of the three sets, model tectonic deformation increments, ${}^i\mathbf{D}_e$, ${}^i\mathbf{D}_n$ and ${}^i\mathbf{D}_w$, can be calculated by means of equation (9). If the mechanical properties of the rocks have a negligible spatial variation, then the pure shear increments, ${}^i\mathbf{U}_e$, ${}^i\mathbf{U}_n$ and ${}^i\mathbf{U}_w$, should also differ only minimally from one set to another. Thus, the most plausible tectonic deformation increments can be obtained by a search for a combination of variables, ${}^g\alpha_e$, ${}^g\alpha_n$, ${}^g\alpha_w$ and x, that minimizes the strain dispersion from set to set.

Table 3 lists five examples of combinations of ${}^g\alpha_e$, ${}^g\alpha_n$ and ${}^g\alpha_w$ used for searches. In each search, the compaction factor, x, was varied from 0.4 to 1 in 10 steps; all five searches gave the lowest strain dispersion at a compaction factor of 0.7 (Fig. 7). Search No. 4 with this compaction factor is the most plausible combination at which the minimal strain dispersion is obtained (Fig. 7 and Table 3). The principal values and directions for the optimal pure shear increments, ${}^i\mathbf{U}_e$, ${}^i\mathbf{U}_n$ and ${}^i\mathbf{U}_w$, are tabulated in Table 4, and Table 5 shows the axes and of the corresponding rigid-body rotations, ${}^i\mathbf{R}_e$, ${}^i\mathbf{R}_n$ and ${}^i\mathbf{R}_w$. Figure 8 shows the geometric relationships of the optimal principal directions of pure shear increments, rotation axes and rotation senses. The axes of maximum elongation point downward and those of greatest shortening are approximately horizontal and, with their NE–SW direction, approximately normal to the fold axis. The rigid-body rotations for the three sets are all clockwise, with rotation axes spread approximately along the principal strain plane normal to the axis of greatest shortening. The W-set, with the steepest average bedding, has the most gently inclined axis. Whereas, the principal directions for the three sets are in close agreement, their principal values differ significantly (Table 4); the pure shear increment for the E-set is of the constriction type, while those for the N- and W-sets are of the flattening type.

Deformation path of the block

The deformation path of the Campbell block, simulated with the proposed incremental deformation model, has 32 progressive states of strain and bedding attitudes for each of the three types of deformation bands. The intermediate states of strain are obtained by equations (12)–(15). The paths for the principal directions are shown in Figs. 9(a)–(c). Whereas each pure shear increment for the N-set, shown as a Flinn plot (Fig. 10), is a flattening strain, the resulting cumulative total strain is of the constriction type. The path of the W-set has a near-reversal. The evolution of the bedding attitudes for each set was calculated with the help of equations (16) and (17), and is plotted in Figs. 11(a)–(c); the orientations of average geometric fold axes for each stage are shown in Fig. 11(d). Figures 9 and 10 demon-

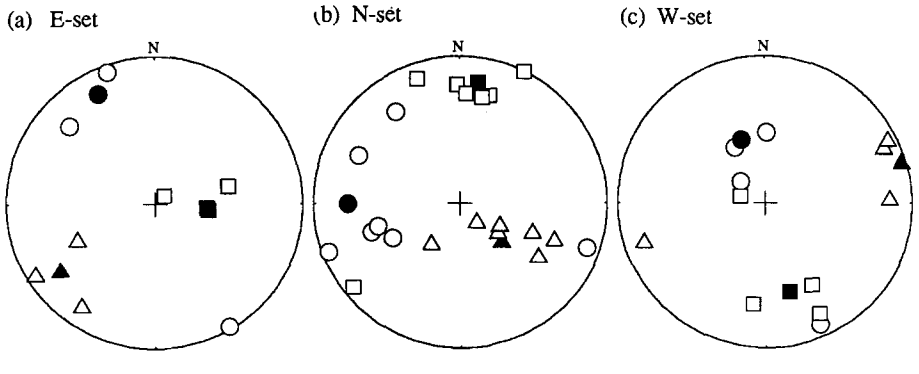

Fig. 5. Synoptic lower-hemisphere equal-area projections of principal strain axes. (a) E-set. (b) N-set. (c) W-set. Squares: maximum; circles: intermediate; triangles: least principal strain directions. Filled squares, circles and triangles: average axes.

Table 1. Principal strain axes and stretch values, s_1, s_2, s_3: maximum, intermediate and least principal stretches

Sample No.	s_1	Trend (°)	Plunge (°)	s_2	Trend (°)	Plunge (°)	s_3	Trend (°)	Plunge (°)
E-set:									
BR-02	1.19	284	76	0.98	156	9	0.85	65	11
CK-01	1.20	77	48	1.07	341	6	0.78	245	42
CK-02	1.26	152	36	1.13	2	50	0.70	253	15
N-set:									
CK-05	1.16	26	1	0.97	296	25	0.89	118	65
CK-06	1.15	232	7	1.12	325	25	0.77	127	64
CK-07	1.15	341	12	1.02	250	5	0.85	137	77
CK-8A	1.14	4	26	0.97	242	47	0.90	111	32
CK-8B	1.23	359	20	1.03	252	37	0.79	111	46
CK-09	1.32	15	26	0.94	109	8	0.81	216	63
CK-10	1.22	12	27	0.96	254	42	0.86	124	36
W-set:									
BR-01	1.20	155	16	1.04	311	72	0.80	63	7
BR-03	1.15	95	61	1.03	313	23	0.84	216	16
CK-03	1.22	188	30	1.08	332	55	0.76	88	17
CK-04	1.17	46	83	1.12	150	2	0.76	240	7

Table 2. Mean principal stretches, directions, and strain dispersions (see text) in the E-, N- and W-sets, s_1: maximum, s_2: intermediate, s_3; least

Set	s_1	Trend (°)	Plunge (°)	s_2	Trend (°)	Plunge (°)	s_3	Trend (°)	Plunge (°)	Strain dispersion
E-set	1.14	97	61	1.06	333	18	0.82	235	23	0.05
N-set	1.17	8	18	0.99	270	24	0.86	131	59	0.05
W-set	1.15	165	37	1.09	339	53	0.80	73	3	0.06

strate that the progressive deformation in the block is heterogeneous. The observed geometric fold axis (Fig. 4) did not act as an axis for rigid-body rotations; it simply coincides approximately with the material line $-{}^{E}\mathbf{l}$ (Fig. 11).

Tectonic implications

As being manifest from the combination of clockwise rotation increments with pure shear increments in the individual deformation bands (Fig. 8), the Campbell block has a non-coaxial deformation style, a combination of progressive simple shear and progressive pure shear components. The fold train was formed within a heterogeneous shear zone. The regional deformation can be partitioned into fairly homogeneous deformation bands with local perturbations. Illustrated with Fig. 12, the deformation bands with the steepest bedding, i.e. those of the W-set, have gently plunging, SE-trending rotation axes; the shearing in these bands displaces rocks in the east over those in the west. The deformation bands represented by the N- and E-sets have steeply plunging rotation axes that facilitate primarily right-lateral shear. Throughout the block, the progressive pure shear component has greatest shortening in NE–SW direction. Combination of these deformation bands sheared the block as a whole in an east-over-west, right-lateral transpression (cf. Harland 1971). This agrees with the observed dip-slip component of the displacement along its boundary faults, the Bear River fault and Mike Ranch thrust, both described as east-over-west backthrusts by Day *et al.* (1985). Should these faults have behaved as stretching faults (Means 1989, 1990), then the formation of the train of folds is interrelated to slip on the faults. The model would then indicate an unobserved dextral strike-slip component of faulting.

The principal directions of pure shear increments of the tectonic deformation, ${}^{i}\mathbf{U}_e$, ${}^{i}\mathbf{U}_n$ and ${}^{i}\mathbf{U}_w$, are approximately consistent throughout the block (Fig. 8). If principal axes of the small strain increments approximately coincide with axes of the contemporaneous stress tensors, the principal directions of the far-field stress during the Nevadan orogeny would be comparable to those of the pure shear increments (Fig. 8).

DISCUSSION

The model consists of two hypothetical deformation paths. The first, a purely conceptual three-step path, is formulated to determine a deformation matrix, or family of deformation matrices, dependent on the constraints provided by observational data. The second, a more realistic incremental deformation path, serves to simulate a steady-state, progressive deformation and to examine its possible style. Generally, the incremental deformation path (equation 5) should be formulated according to the kind of strain measurement used in each study. For instance, had the strain **S** been determined by ellipsoidal markers that had changed shape by a tectonic strain only, then the compaction step **C** in equation (5) should have been omitted.

The model accounts for deformation in the straight limbs of the fold train and leaves out the hinge areas where a complicated strain field is present. The folding

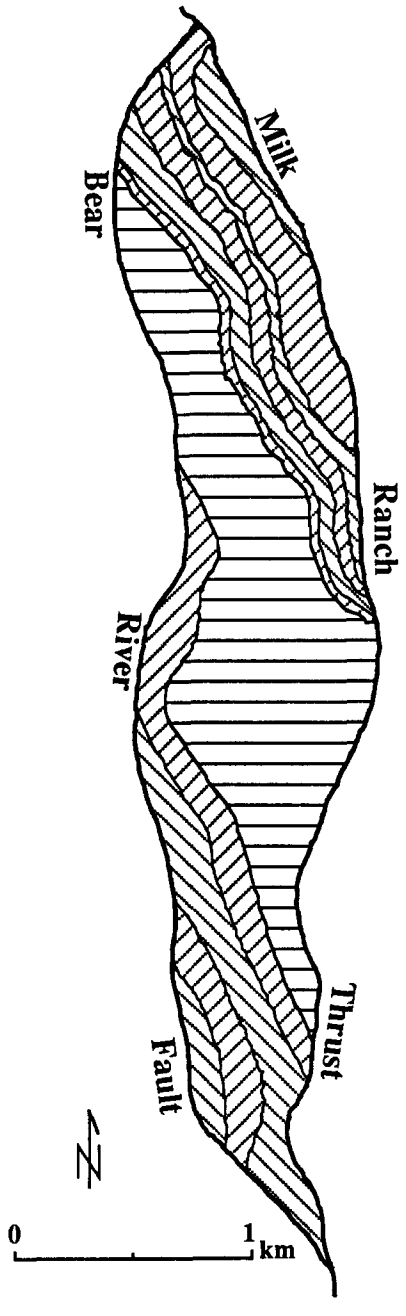

Fig. 6 Division of the Campbell block into deformation bands. The bands are separated by the axial traces of the folds (see Fig. 3). Horizontal ruling: N-set type. Slash ruling: E-set type. Back-slash ruling: W-set type.

kinematics of the entire fold train is consequently approximated by the deformation paths of its limbs. This approximation should be close to actual folding kinematics, if the fold axes did not roll over laterally and if the

Table 3. Combinations of rotation angles ${}^{g}\alpha$ in the E-, N- and W-sets, and lowest strain dispersions for searches Nos 1–5

Search	${}^{g}\alpha_e$	${}^{g}\alpha_n$	${}^{g}\alpha_w$	Lowest strain dispersion
1	0	0	0	0.001500
2	80	40	30	0.001236
3	115	65	50	0.001151
4	115	60	50	0.001139
5	125	75	60	0.001171

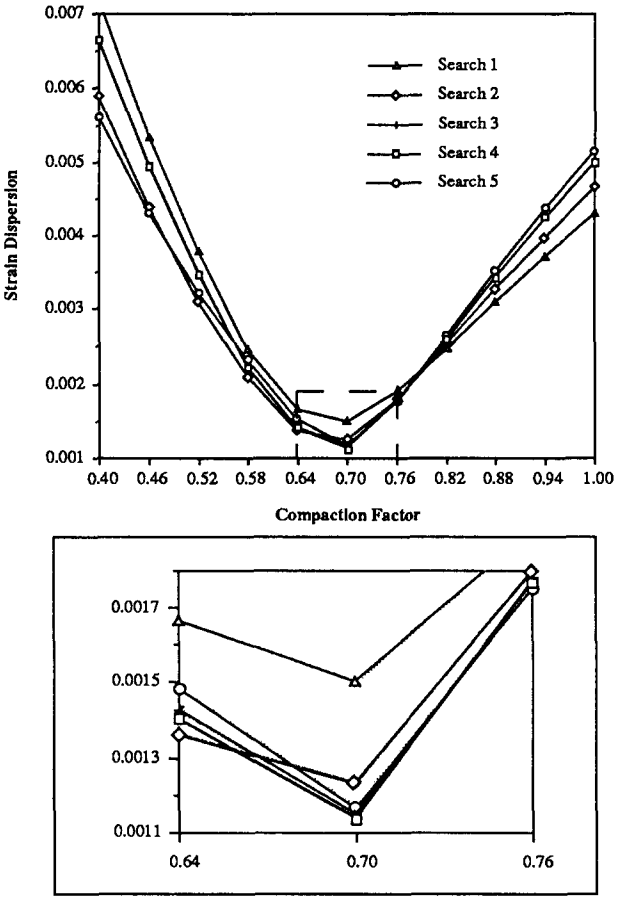

Fig. 7. Variation of strain dispersion with compaction factor, x, changing from 0.4 to 1.0 in 10 steps, for searches Nos 1–5. Insert: magnified portion of diagram for compaction factors from 0.64 to 0.76.

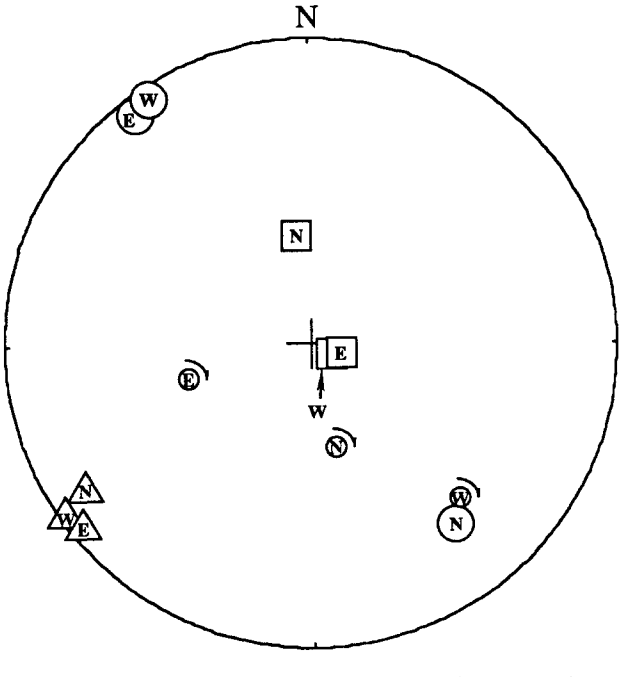

Fig. 8. Synoptic lower-hemisphere equal-area projection of principal axes of optimal pure shear increments and of rigid-body rotation axes for E-, N- and W-sets. Symbols for principal directions as in Fig. 5. Circles with sense of rotation: rotation axes.

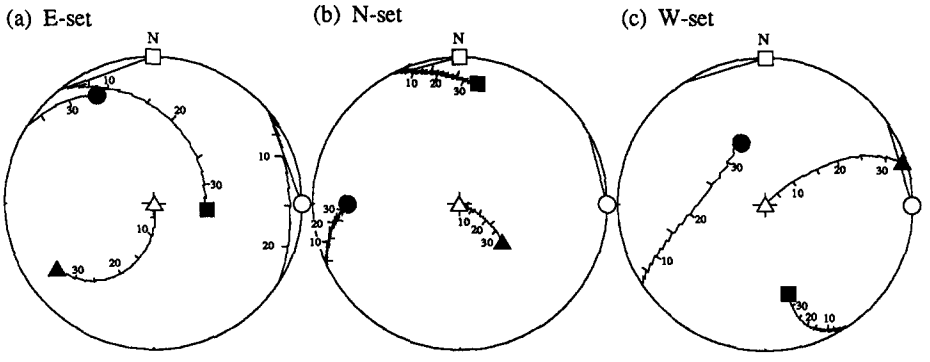

Fig. 9. Synoptic lower-hemisphere equal-area projections of progressive displacement of principal axes during intermediate-stage strains. (a) E-set. (b) N-set. (c) W-set. Open symbols (as in Fig. 5): first stage after compaction; equal 'maximum' and 'intermediate' directions arbitrarily shown at present geographic north and east. Filled symbols: axes of present average March strains. Numbers: deformation stages.

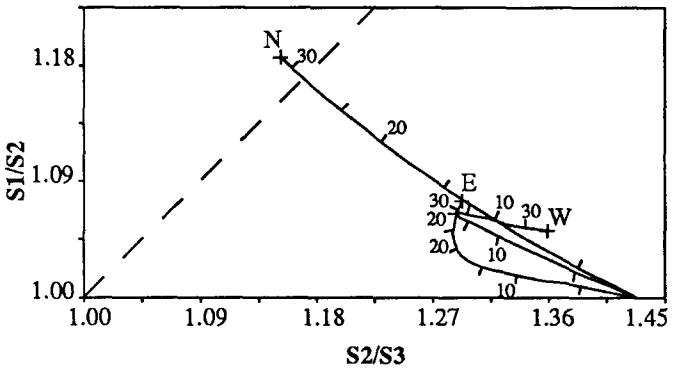

Fig. 10. Flinn plot of deformation paths for E-, N- and W-sets. Numbers: deformation stages. Dashed line: plane-strain line.

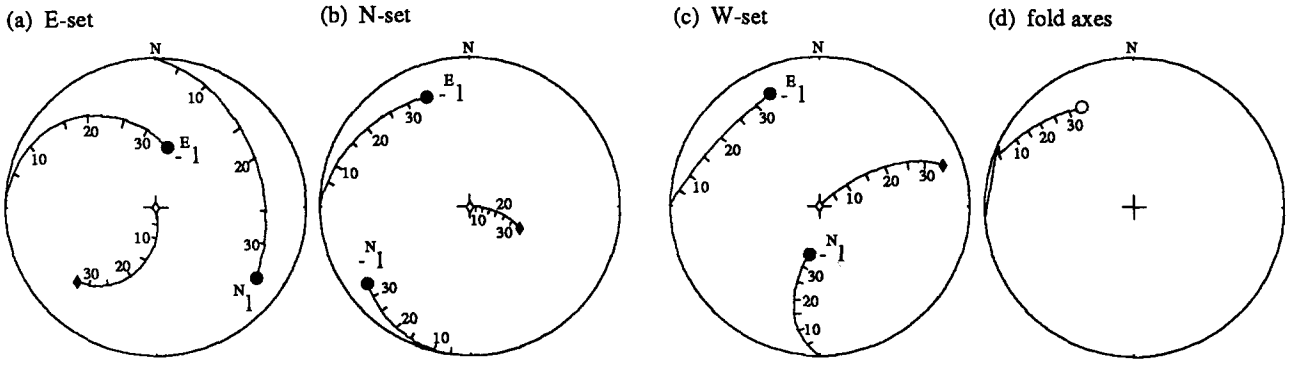

Fig. 11. Synoptic lower-hemisphere equal-area projections of progressive line orientations. Orientations of bedding poles and of material lines initially parallel to the present geographic north, $^{N}\mathbf{1}$, and east, $^{E}\mathbf{1}$. (a) E-set. (b) N-set. (c) W-set. Open diamonds: initial bedding poles; filled diamonds: present bedding poles. Filled circles: material lines. Numbers: deformation stages. (d) Orientations of fold axes, calculated from progressive bedding poles of the three sets. Open circles: calculated apparent fold axes. Numbers: deformation stages.

amplification of the fold train was achieved primarily by rigid-body rotations and stretches of its limbs. The most plausible deformation path of the fold train is obtained by assuming minimal spatial variation of the rheology in the fold train. This assumption is supported by the results of the fitting. Among the three sets, the optimal fit yields close coincidence of the principal directions of the incremental strain field (Fig. 8) which may indicate the principal directions of the far-field stress imposed on the entire fold train. The inferred maximum compression direction is perpendicular to the common fold axes.

Pure shear and rigid-body rotation increments could

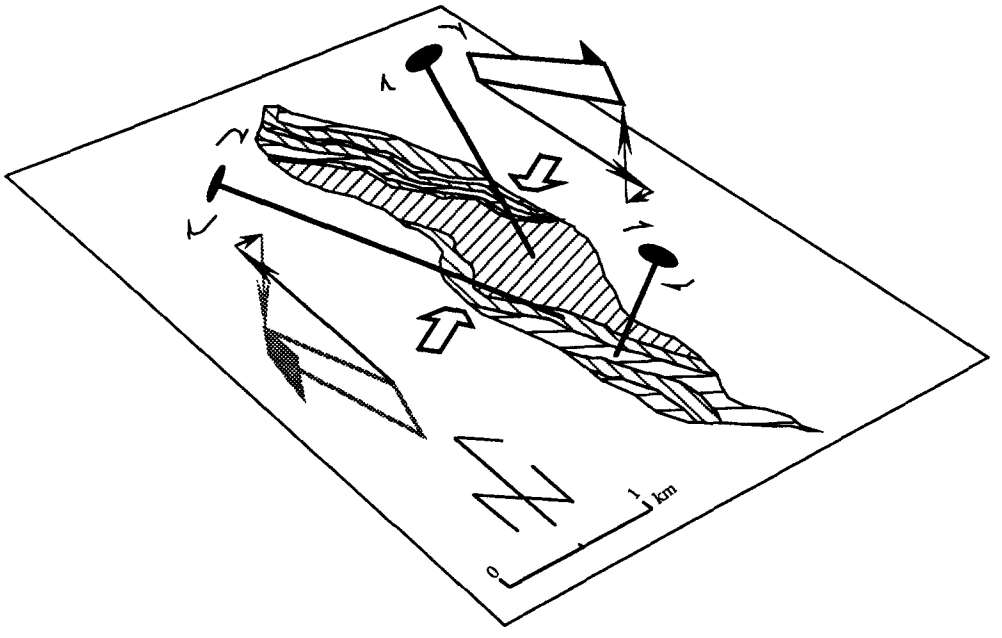

Fig. 12. Diagrammatic representation of deformation components of the Campbell block (details see text). Three inclined axis with sense arrows indicate the incremental rotation axes for three types of deformation bands. Open arrows indicate the greatest shortening direction shared by 11 deformation bands. The half arrows decorated with their vector components qualitatively show, as a whole, an east-over-west, right-lateral transpression. Division patterns of the Campbell block as in Fig. 6.

Table 4. Principal incremental pure shear stretches and directions of principal stretches for the E-, N- and W-sets. u_1, u_2, u_3: maximum, intermediate and least principal stretches

Set	u_1	Trend (°)	Plunge (°)	u_2	Trend (°)	Plunge (°)	u_3	Trend (°)	Plunge (°)
E-set	1.007972	106	82	0.997851	323	6	0.994228	232	5
N-set	1.009445	353	61	1.000116	142	25	0.990529	238	13
W-set	1.007501	114	84	1.000802	327	5	0.991760	237	3

be calculated only as averages for the deformation bands; local perturbations had to be neglected. Because strains were measured only in the shale interlayers of a shale–siltstone succession, and because shales are presumably the less competent of the two, the calculated deformation matrices may be taken as upper limits for the deformation of the block as a whole.

CONCLUSIONS

A conceptual deformation matrix can be formulated by setting up a simple hypothetical three-step deformation path. A procedure that extracts the square-root of a matrix provides a means to factorize this deformation matrix into small equal increments, which simulate the progressive deformation of a rock. The calculated deformation path assumes a rock deformed under steady-state conditions. As shown in the example of the Campbell block, the incremental deformation model, combined with the concept of deformation bands, allows the study of a heterogeneously deformed region. The nature of deformation in that region was examined by polar decomposition of each increment and by finding the eigenvalues and eigenvectors of each pure shear increment, and the axis and angle of each rigid-body rotation increment. It was found that the deformation style of the block contains a simple shear component. The regional strain is accommodated among the several deformation bands by strain partition; the collective deformation indicated by this model is transpressional.

Table 5. Orientation of rotation axes and angles of optimal rigid-body rotations in the E-, N- and W-sets

Set	Trend (°)	Plunge (°)	Amount of rotation
E-set	256	56	7.76
N-set	168	62	4.14
W-set	136	31	5.29

Acknowledgements—I thank J. Christie, P. Cobbold, W. Dollase, B. Ildefonse, C. Passchier and G. Oertel for advice on the manuscript, B. Hacker for introducing me to the Colfax Sequence, and R. Alkaly for preparing thin sections for the X-ray goniometer.

REFERENCES

Biot, M. A. 1961. Theory of folding of stratified viscoelastic media and its implications in tectonics and orogenesis. *Bull. geol. Soc. Am.* **72**, 1595–1620.

Borradaile, G. J. 1991. Remanent magnetism and ductile deformation

in an experimentally deformed magnetite-bearing limestone. *Phys. Earth & Planet. Interiors* **67**, 362–373.
Borradaile, G. J. & Mothersill, J. S. 1991. Experimental strain of isothermal remanent magnetization in ductile sandstone. *Phys. Earth & Planet. Interiors* **65**, 308–318.
Burchfiel, B. C. & Davis, G. A. 1975. Nature and controls of Cordilleran orogenesis, western United States: Extensions of an earlier synthesis. *Am. J. Sci.* **275A**, 363–396.
Burnett, J. L. & Jennings, C. W. 1962. *Chico Sheet*; *Geologic map of California*: scale 1:250,000. California Division of Mines and Geology.
Chandra, D. K. 1961. *Geology and Mineral Deposits of the Colfax and Foresthill Quadrangles, California*. California Division of Mines, Special Report 67.
Chen, R. T. & Oertel, G. 1989. Strain history of the Los Prietos syncline, Santa Maria basin, California: a case of post-tectonic compaction. *J. Struct. Geol.* **11**, 539–551.
Chen, R. T. & Oertel, G. 1991. Determination of March strain from phyllosilicate preferred orientation: A semi-numerical method. *Tectonophysics* **200**, 173–185.
Cobbold, P. R. 1977. Description and origin of banded deformation structures. I. Regional strain, local perturbations, and deformation bands. *Can. J. Earth Sci.* **14**, 1721–1731.
Cogné, J. P. & Perroud, H. 1985. Strain removal applied to paleomagnetic direction in an orogenic belt: the Permian red slates of the Alpes Maritimes, France. *Earth Planet. Sci. Lett.* **72**, 125–140.
Cogné, J. P. & Perroud, H. 1987. Unstraining paleomagnetic vectors: the current state of debate. *Eos* **68**, 711–712.
Coward, M. P. & Potts, G. J. 1983. Complex strain patterns developed at the frontal and lateral tips to shear zones and thrust zones. *J. Struct. Geol.* **5**, 383–399.
Day, H. W., Moores, E. M. & Tuminas, A. C. 1985. Structure and tectonics of the northern Sierra Nevada. *Bull. geol. Soc. Am.* **96**, 436–450.
Durney, D. W. & Ramsay, J. G. 1973. Incremental strains measured by syntectonic crystal growths. In: *Gravity and Tectonics* (edited by De Jong, K. A. & Scholten, R.). Wiley, New York, 67–96.
Elliott, D. 1970. Determination of finite strain and initial shape from deformed elliptical objects. *Bull. geol. Soc. Am.* **81**, 2221–2236.
Elliott, D. 1972. Deformation paths in structural geology. *Bull. geol. Soc. Am.* **83**, 2621–2638.
Ellis, M. & Watkinson, A. J. 1987. Orogen-parallel extension and oblique tectonics: The relation between stretching lineations and relative plate motions. *Geology* **15**, 1027–1030.
Fletcher, R. C. 1982. Coupling of diffusional mass transport and deformation in a tight rock. *Tectonophysics* **83**, 275–291.
Flinn, D. 1962. On folding during three-dimensional progressive deformation. *Q. J. geol. Soc. Lond.* **118**, 385–433.
Flinn, D. 1979. The deformation matrix and the deformation ellipsoid. *J. Struct. Geol.* **1**, 299–307.
Hamilton, W. 1969. Mesozoic California and the underflow of the Pacific mantle. *Bull. geol. Soc. Am.* **80**, 2409–2430.
Harper, G. D., Saleeby, J. B. & Norman E. A. S. 1985. Geometry and tectonic setting of sea-floor spreading for the Josephine ophiolite, and implications for Jurassic accretionary events along the California margin. In: *Tectonostratigraphic Terrances of the Circum-Pacific Region* (edited by Howell, D. G.). Circum-Pacific Council for Energy and Mineral Resources, Houston, 239–258.
Harland, W. B. 1971. Tectonic transpression in Caledonian Spitsbergen. *Geol. Mag.* **108**, 27–42.
Imlay, R. W. 1961. Late Jurassic ammonites from the western Sierra Nevada, California. *Prof. Pap. U.S. geol. Surv.* **374D**, D1–D30.
Ingersoll, R. V. & Schweickert, R. A. 1986. A plate-tectonic model for Late Jurassic ophiolite genesis, Nevadan orogeny and forearc initiation, northern California. *Tectonics* **5**, 901–912.
Johnson, A. M. & Ellen, S. D. 1974. A theory of concentric, kink, and sinusoidal folding and of monoclinal flexuring of compressible, elastic multilayers. I. Introduction. *Tectonophysics* **21**, 301–339.
MacDonald, W. D. 1980. Net tectonic rotation, apparent tectonic rotation, and the structural tilt correction in paleomagnetic studies. *J. geophys. Res.* **85**, 3659–3669.
March, A. 1932. Mathematische Theorie der Regelung nach der Korngestalt bei Affiner Deformation. *Z. Kristallogr.* **81**, 285–297.
McKenzie, D. & Jackson, J. 1983. The relationship between strain rates, crustal thickening, paleomagnetism, finite strain and fault movements within a deformation zone. *Earth Planet. Sci. Lett.* **65**, 182–202.
Means, W. D. 1989. Stretching faults. *Geology* **17**, 893–896.
Means, W. D. 1990. One-dimensional kinematics of stretching faults. *J. Struct. Geol.* **12**, 267–272.
Means, W. D., Hobbs, B. E., Lister, G. S. & Williams, P. F. 1980. Vorticity and non-coaxiality in progressive deformations. *J. Struct. Geol.* **2**, 371–378.
Moores, E. M. 1972. Ultramafics and orogeny, with models of the U.S. Cordillera and Tethys. *Nature, Lond.* **228**, 837–842.
Moores, E. M. & Day, H. W. 1984. Overthrust model for the Sierra Nevada. *Geology* **12**, 416–419.
Nye, J. F. 1957. *Physical Properties of Crystals*. Oxford University Press, London.
Odling, N. E. 1984. Strain analysis and strain path modelling in the Loch Tollie gneisses, Gairloch, NM Scotland. *J. Struct. Geol.* **6**, 543–562.
Oertel, G. 1983. The relationship of strain and preferred orientation of phyllosilicate grains in rocks: A review. *Tectonophysics* **100**, 413–447.
Oertel, G., Engelder, T. & Evans, K. 1989. A comparison of the strain of crinoid columnals with that of their enclosing silty and shaly matrix on the Appalachian Plateau, New York. *J. Struct. Geol.* **11**, 975–993.
Owens, W. H. 1973. Strain modification of angular density distributions. *Tectonophysics* **16**, 249–261.
Passchier, C. W. 1987. Stable positions of rigid objects in non-coaxial flow—a study in vorticity analysis. *J. Struct. Geol.* **9**, 679–690.
Ramberg, H. 1975. Particle paths, displacement and progressive strain applicable to rocks. *Tectonophysics* **28**, 1–37.
Ramberg, H. & Ghosh, S. K. 1977. Rotation and strain of linear and planar structures in three-dimensional progressive deformation. *Tectonophysics* **40**, 309–337.
Ramsay, J. G. 1967. *Folding and Fracturing of Rocks*. McGraw-Hill, New York.
Ramsay, J. G. & Huber, M. I. 1983. *The Techniques of Modern Structural Geology, Volume* 1: *Strain Analysis*. Academic Press, London.
Saleeby, J. B., Goodin, S. E., Sharp, W. D. & Busby, C. J. 1978. Early Mesozoic paleotectonic–paleogeographic reconstruction of the southern Sierra Nevada region. In: *Mesozoic Paleogeography of the Western United States* (edited by Howell, D. G. & Mcdougall, K. A.). *Pacific Coast Paleogeography Symposium* 2, *Soc. econ. Paleont. Miner. Pacific Sec.* 311–336.
Sanderson, D. J. & Marchini, W. R. D. 1984. Transpression. *J. Struct. Geol.* **6**, 449–458.
Scheidegger, A. E. 1965. On the statistics of the orientation of bedding planes, grain axes and similar sedimentological data. *Prof. Pap. U.S. geol. Surv.* **525**, C164–C167.
Schultz-Ela, D. D. & Hudleston, P. J. 1991. Strain in an Archean greenstone belt of Minnesota. *Tectonophysics* **190**, 233–268.
Schweickert, R. A. & Cowan, D. S. 1975. Early Mesozoic tectonic evolution of the western Sierra Nevada, California. *Bull. geol. Soc. Am.* **86**, 1329–1336.
Schwerdtner, W. M. & Gapais, D. 1983. Calculation of finite incremental deformations in ductile geological materials and structural models. *Tectonophysics* **93**, T1–T7.
Spencer, A. J. M. 1980. *Continuum Mechanics*. Longman, New York.
Shore, P. J. & Duncan, I. J. 1984. Finite strains from non-coaxial strain paths. I. computational techniques. *Tectonophysics* **110**, 127–144.
Tuminas, A. C. 1983. Geology of the Grass Valley–Colfax region, Sierra Nevada, California. Unpublished Ph.D. dissertation, University of California, Davis.
Wagner, D. L., Jennings, C. W., Bedrossian, T. L. & Bortugno, E. J. 1981. *Geologic map of the Sacramento Quadrangle, California*: *California Division of Mines and Geology, Regional Map Series Map No. 1A*, scale 1:250,000.
Wenk, H. -R. 1985. Measurement of pole figures. In: *Preferred Orientation in Deformed Metals and Rocks: An Introduction to Modern Texture Analysis* (edited by Wenk, H.-R.). Academic Press, Orlando, 11–47.

APPENDIX A

FORMULATION AND ANALYSIS OF A ROTATION MATRIX

A rotation matrix, $\mathbf{Q} = Q_{ij}$, represents a rigid-body rotation process; it has the properties of an orthogonal matrix:

$$\mathbf{Q}^{-1} = \mathbf{Q}^{\mathrm{T}}; \tag{A1}$$

and

$$|\mathbf{Q}| = 1; \quad \text{or} \quad 1 = e_{ijk}Q_{1i}Q_{2j}Q_{3k}, \tag{A2}$$

where e_{ijk} is the alternating matrix. The process rotates a body rigidly through an angle α clockwise about an axis pointing in the direction of a unit vector $\mathbf{n}$ with components n_i. The rotation matrix $\mathbf{Q}$ has the following components (equations 6.11 in Spencer 1980):

$$Q_{ir} = \delta_{ir}\cos\alpha + e_{ijr}n_j\sin\alpha + (1 - \cos\alpha)n_in_r, \tag{A3}$$

where δ_{ij} is the identity matrix. By inversion of equation (A3), a given rotation matrix $\mathbf{Q}$ with components Q_{ir} represents a rotation about the axis $\mathbf{n}$ through the angle α:

$$n_k = \frac{e_{ikj}Q_{ij}}{(e_{rij}Q_{if}e_{rpq}Q_{pq})^{1/2}}; \tag{A4}$$

and

$$\alpha = \cos^{-1}\frac{(\delta_{ij}Q_{ij} - 1)}{2}. \tag{A5}$$

Hence, the operation of a rotation matrix can be analysed by means of equations (A4) and (A5).

APPENDIX B

EXTRACTING THE 'SQUARE-ROOT' OF A MATRIX

In analogy with the scalar case, a matrix, ${}^{\mathrm{r}}\mathbf{H}$, is defined as the *square-root* of another matrix, $\mathbf{W}$, which is the product of self-multiplication of the matrix, ${}^{\mathrm{r}}\mathbf{H}$, i.e.:

$$\mathbf{W} = {}^{\mathrm{r}}\mathbf{H}\,{}^{\mathrm{r}}\mathbf{H}. \tag{B1}$$

In the existing literature on matrix algebra, there has been discussion of the properties of the 'square-root' for symmetric matrices but not for asymmetric matrices. It exceeds the scope of this paper to delimit the existence and uniqueness conditions for such a matrix or to attempt its general analytic solution. To obtain ${}^{\mathrm{r}}H_{ij}$ from a given 3×3 matrix W_{ij}, one has to solve a set of nine simultaneous non-linear equations. Instead, I propose an iterative numerical solution.

Let matrices $\mathbf{W}$ and ${}^{\mathrm{r}}\mathbf{H}$ have components as follows:

$$(W_{ij}) = \begin{bmatrix} W_{11} & W_{12} & W_{13} \\ W_{21} & W_{22} & W_{23} \\ W_{31} & W_{32} & W_{33} \end{bmatrix} \tag{B2}$$

and

$$({}^{\mathrm{r}}H_{ij}) = \begin{bmatrix} {}^{\mathrm{r}}H_{11} & {}^{\mathrm{r}}H_{12} & {}^{\mathrm{r}}H_{13} \\ {}^{\mathrm{r}}H_{21} & {}^{\mathrm{r}}H_{22} & {}^{\mathrm{r}}H_{23} \\ {}^{\mathrm{r}}H_{31} & {}^{\mathrm{r}}H_{32} & {}^{\mathrm{r}}H_{33} \end{bmatrix}. \tag{B3}$$

Express (B1) with indices, subject to the Einstein summation convention:

$$W_{ij} = {}^{\mathrm{r}}H_{ik}\,{}^{\mathrm{r}}H_{kj}. \tag{B4}$$

Let a tentative square-root matrix, $\mathbf{H}$, have components H_{ij}. They deviate from the components of the true square-root matrix, ${}^{\mathrm{r}}\mathbf{H}$, by small 'square-root deviations', δH_{ij}, thus:

$${}^{\mathrm{r}}H_{ij} = H_{ij} + \delta H_{ij}. \tag{B5}$$

Substituting (B5) into (B4), it becomes:

$$W_{ij} = (H_{ik} + \delta H_{ik})(H_{kj} + \delta H_{kj}). \tag{B6}$$

The deviations of the product components of self-multiplication of the tentative matrix, $\mathbf{H}$, from those of the given matrix, $\mathbf{W}$, can be calculated as the 'product discrepancies', ΔW_{ij}:

$$\Delta W_{ij} = W_{ij} - H_{ik}H_{kj}. \tag{B7}$$

Rearranging the terms of (B7), one obtains:

$$W_{ij} = H_{ik}H_{kj} + \Delta W_{ij}. \tag{B8}$$

Substituting (B6) into (B8), it becomes:

$$(H_{ik} + \delta H_{ik})(H_{kj} + \delta H_{kj}) = H_{ik}H_{kj} + \Delta W_{ij}, \tag{B9}$$

and therefore

$$H_{ik}\delta H_{kj} + \delta H_{ik}H_{kj} + \delta H_{ik}\delta H_{kj} = \Delta W_{ij}. \tag{B10}$$

Because the square-root deviations, δH_{ij}, are comparatively small, in a numerical approximation the terms $\delta H_{ik}\delta H_{kj}$ can be ignored. Equation (B13) can thus be linearized as:

$$H_{ik}\delta H_{kj} + \delta H_{ik}H_{kj} = \Delta W_{ij}. \tag{B11}$$

Equation (B11) represents a set of nine simultaneous equations, which in matrix form are:

$$\mathbf{A}\ \mathbf{x} = \mathbf{b}, \tag{B12}$$

where $\mathbf{A}$ is the matrix of coefficients:

$$\mathbf{A} = \begin{bmatrix} H_{11}+H_{11} & H_{21} & H_{31} & H_{12} & 0 & 0 & H_{13} & 0 & 0 \\ H_{12} & H_{11}+H_{22} & H_{23} & 0 & H_{12} & 0 & 0 & H_{13} & 0 \\ H_{13} & H_{23} & H_{11}+H_{33} & 0 & 0 & H_{12} & H_{31} & 0 & H_{13} \\ H_{21} & 0 & 0 & H_{22}+H_{11} & H_{21} & H_{31} & H_{23} & 0 & 0 \\ 0 & H_{21} & 0 & H_{12} & H_{22}+H_{22} & H_{32} & 0 & H_{23} & 0 \\ 0 & 0 & H_{21} & H_{13} & H_{21} & H_{33}+H_{22} & 0 & 0 & H_{23} \\ H_{31} & 0 & 0 & H_{32} & 0 & 0 & H_{33}+H_{11} & H_{21} & H_{31} \\ 0 & H_{31} & 0 & 0 & H_{32} & 0 & H_{12} & H_{33}+H_{22} & H_{32} \\ 0 & 0 & H_{31} & 0 & 0 & H_{32} & H_{13} & H_{23} & H_{33}+H_{33} \end{bmatrix}. \tag{B13}$$

Consider the left-hand column vector in equation (B12), $\mathbf{x}$, formed by the nine square-root deviations, δH_{ij}, as the unknown with the known column vector, $\mathbf{b}$, formed by the nine product discrepancies, ΔW_{ij}, on the right-hand side. The unknown vector $\mathbf{x}$ can be found by Cramer's rule, if the coefficient matrix $\mathbf{A}$ is non-singular. Because of the linearization of equation (B11), equation (B5) is rewritten as:

$${}^{\mathrm{r}}H_{ij} \approx {}^{\mathrm{a}}H_{ij} = H_{ij} + \delta H_{ij}. \tag{B14}$$

The tentative square-root matrix $\mathbf{H}$ can be recalculated now by using equation (B14). The components of the refined matrix, ${}^{\mathrm{a}}H_{ij}$, in the next iteration approach more closely those of the true square-rooted matrix ${}^{\mathrm{r}}\mathbf{H}$. By iterated solution of equation (B12) and substituting the results into equations (B14) and (B7), one can obtain a square-root matrix to within any desired precision. In the current study, the extracting procedure was programmed in Pascal run on Macintosh II. By five or six iterations, the values of square-root deviations, δH_{ij}, can be reduced to an order of 10^{-12}.